Chapter 9
Interfacial Materials for Efficient Solution Processable Organic Photovoltaic Devices

Chang-Zhi Li, Hin-Lap Yip and Alex K.-Y. Jen

Abstract The introduction of proper interfacial materials to optimize properties between organic/metal and organic/organic interfaces has become an important criterion to improve the performance and stability of polymer solar cells. This chapter presents an overview on the recent development of effective interfacial materials (including organic, inorganic and hybrid materials) used for both organic/metal and organic donor/acceptor interface engineering, and the integration of these materials in different device architectures to enhance efficiency and stability are also discussed.

9.1 Introduction

Aiming for solar energy harvest, photovoltaic technology exhibited its promise for meeting the urgent demand for clean and renewable energy, of which both inorganic and organic PVs attracted extensive research efforts. As the one of most abundant renewable energy source, solar energy is as high as 120,000 TW accounting for sunlight reaches to the earth surface per year (far beyond the global energy demand $\sim$15 TW/year) [1]. Photovoltaic research is therefore extremely motived to tackle energy problem by pursuing efficient conversion of solar energy into electricity. In the past two decades, organic photovoltaics (OPVs) processing their extra merits (to inorganic one) of mechanical flexibility, light-weight, and large scale processability, have experienced rapid development [2, 3]. One may be impressed by the significant progress on improving the performance of OPVs with power conversion efficiencies (PCE) from 1 % [4] to state-of-the-art 8–9 % [5, 6] and achieving in-depth understanding of the physics. Material development always drives the progress of OPV technology. Along with the research on the design and

C.-Z. Li · H.-L. Yip · A.K.-Y. Jen (✉)
Department of Materials Science and Engineering, University of Washington, Seattle, WA, USA
e-mail: ajen@u.washington.edu; ajen@uw.edu

Y. Yang and G. Li (eds.), *Progress in High-Efficient Solution Process Organic Photovoltaic Devices*, Topics in Applied Physics 130,
DOI 10.1007/978-3-662-45509-8_9

processing of active materials [7–12], tremendous efforts have been made on the creation and introduction of proper interfacial materials to optimize properties of interfaces in OPV, which have become important criterion to influence the performance and stability of devices. Recent successful examples demonstrated that engineering of interface is equally important to the efforts on optimizing active materials and processing to get device tuned to obtain maxim achievable performance.

From the device architecture point of view, OPVs usually sandwich a layer of donor and acceptor between a transparent electrode and metal electrode. Basing on electrode polarity of device, basic device architecture divided into conventional and inverted structures (Fig. 9.2). Critical interfaces involving organic/electrode and organic/organic junction were therefore created in device, the quality of which significantly influence (or determine) overall device performance. Electron (ESL) and hole (HSL) selective layer were required to optimize organic/electrode interface and to improve charge extraction efficiency and selectivity of electrode [13–18]. For instance, PEDOT:PSS is commonly used HSL and LiF/Al and Ca/Al used for top cathode to ensure effective charge extraction and maximizing achievable Voc. Another important interface is organic/organic interface created from the heterojunction of donor and acceptor in active layer. Different from the inorganic components, organic semiconductors are excitonic materials generate tightly bonded electron–hole pairs (excitons) upon photo excitation, since their inherent low dielectric constant (usually, $\varepsilon_r =$ 2–4), which require screening force to overcome the binding energy of excitons (for the Frenkel exciton in the range of 0.3–1 eV) to dissociate excitons into free charges. Organic donor/acceptor junction allow providing energy offset at their interface, where became most important interface involving charge separation and recombination, thus directly influence charge photogeneration and photovoltage of device.

In this chapter, we provide an overview of the recent progress on organic/electrode and donor/acceptor interface engineering, as well as the innovation of the related material. Some design criteria and the functions of interfacial layers for efficient OPVs are summarized. Regarding to organic/electrode interface, several classes of interfacial materials integrating high-performance OPVs are highlighted, which including metal oxides, cross linkable charge-transporting materials, conjugated semiconductor electrolytes, self-assembled functional molecules and graphene-based interface materials. It is worthy to note that fundamental understanding of the surface and interface science, and the device physics associated with the interfaces of OPVs is equally important and in-depth discussions on these areas can be found in several review articles [19–24]. Some recent studies involved donor/acceptor interface engineering through insertion of dipole layers for optimizing contact and examples for selective load of fullerene-thiophene hybrids into donor/acceptor interface are also summarized.

OPV device operation and performance evaluation can be briefly described as following: under illumination, excitons will be generated from light-absorbed semiconductors, which then diffused to donor–acceptor interface and dissociate with the assistance of energy offset between donor and acceptors. The separated

charges will then drift under the inherent electric field created by the work-function difference between the asymmetric electrodes, and ultimately, will be collected by the corresponding electrodes. The PCE of OPV is defined by the product of three parameters including short-circuit current density (J_{sc}), open-circuit voltage (V_{oc}), and fill factor (FF). J_{sc} is directly related to the efficiencies of light absorption, exciton generation and dissociation, charge transport and charge collection at the electrodes. V_{oc} is related to the difference between the highest occupied molecular orbital (HOMO) of the donor and the lowest unoccupied molecular orbital (LUMO) of the acceptor in the BHJ. More specifically, it is determined by the difference between the quasi-Fermi levels of holes ($E_{F,h}$) and electrons ($E_{F,e}$) under illumination provided that barrierless contacts to the electrodes are formed (Fig. 9.1) [21, 25]. FF is governed by both the parasitic series resistance (R_s) and shunt resistance (R_p) of the solar cell [26, 27]. R_s is determined by the bulk conductivity of the electrodes, active and interfacial layers, and the contact resistance between them. R_p is determined by the quality of the thin films and their interfaces. Small R_p originates from the loss of charge carriers through leakage paths including pinholes in the films and the recombination and trapping of the carriers during their transit through the cell that can lead to decreased device performance. The nature of electrical contact between the BHJ layer and the electrodes can significantly affect all three device-related parameters and modification of those interfaces by inserting appropriate interfacial layers can significantly alter the contact properties to improve the PCE of OPVs. The donor/acceptor interface affects exciton collection and dissociation, which determined charge photogeneration and photovoltage of device. Engineering of those interfaces through application of appropriate interfacial material can significantly alter the contact and photo physic processes of device leading to improve the performance and stability of OPVs.

9.1.1 Donor/Acceptor Interface

The heterojunction of donor and acceptor in active blend created large area of D/A interface, where excitons get collected and dissociated, thus influence overall device performance. In this section, some of the studies related to donor/acceptor interface engineering with proper interfacial material are introduced and the advance in design criteria is also discussed. As demonstrated by Durrant et al. schematic illustration of charge dissociation at the polymer:PCBM interface is shown in Fig. 9.2. The donor singlet exciton diffuses to the interface, and subsequently generate the charge-transfer (CT) state (Fig. 9.3) at donor/acceptor interface. Exciton itself processes limited lifetime and diffusion length ($\sim$10–20 nm). The one created far away from the interface would relax itself to the ground state without photocurrent contribution. At the CT state, initial electron-hole separation has a distance of the thermalization length (a). The probability of full dissociation into the free charge carriers (the CS state, Fig. 9.3) depends upon the ratio between distance (a) and the coulomb capture radius.

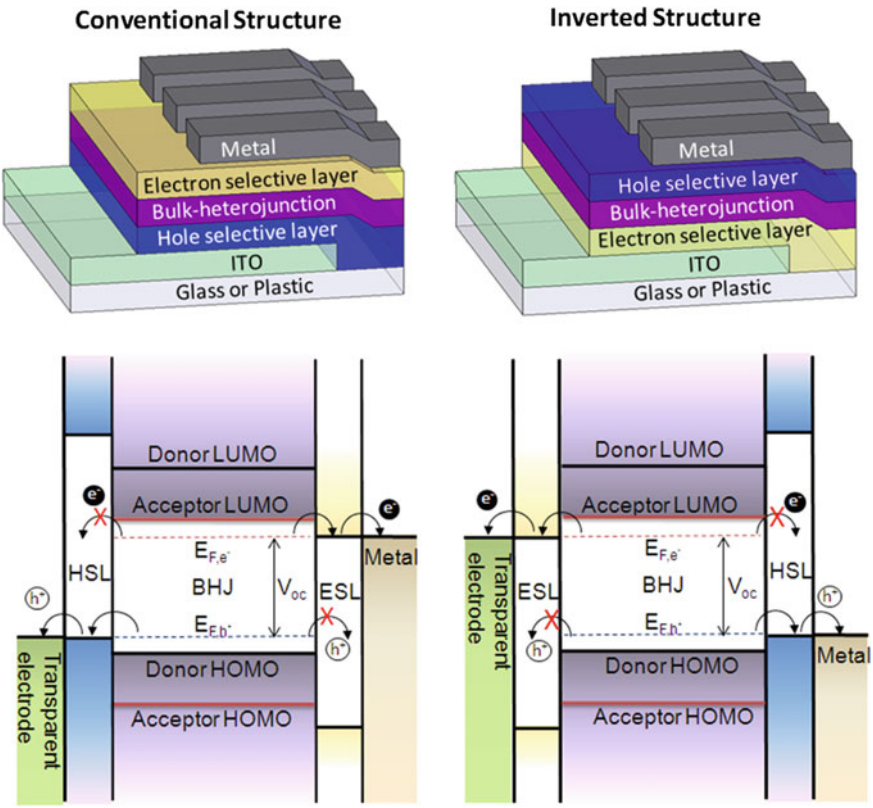

Fig. 9.1 Device architecture of conventional OPV (*upper left*) and inverted OPV (*upper right*). Schematic view of the energy level alignment in a conventional OPV (*bottom left*) and an inverted OPV (*bottom right*) with interfacial layers providing Ohmic contacts and charge selectivity at both electrodes

Charge photogeneration at donor/acceptor interface is one of the most important processes in OPV device. As shown in Fig. 9.4 [26, 28], the singlet exciton generated upon photo excitation of light-absorption semiconductor, which pumped an electron from grand state S_0 into S_1. The exciton then diffused to the interface, where hot charge transfer state, CT* can dissociate into a fully charge-separated (CS) state (K_{CS*}) and migrate away from the D/A interface. This process compete with the thermal relaxation of CT* to CT state (K_{therm}^{CT}). It worthy to note that conjugated materials usually present strong electron-vibration coupling, thus promote relaxing excited state down to the lowest energy level of excited state. At CT state, significant energy loss pathway involved. One is recombination ($K_{triplet}$) of the ^{3}CT (^{1}CT to ^{3}CT, K_{ISC}) to the triplet state of semiconductors, T_1. Another is decay of the ^{1}CT back to the ground state through geminate recombination. Dissociation of the thermally relaxed CT state into the CS state (K_{CS*}) is achieved with the assistance of interfacial energy offset. The diffusion-limited bimolecular process

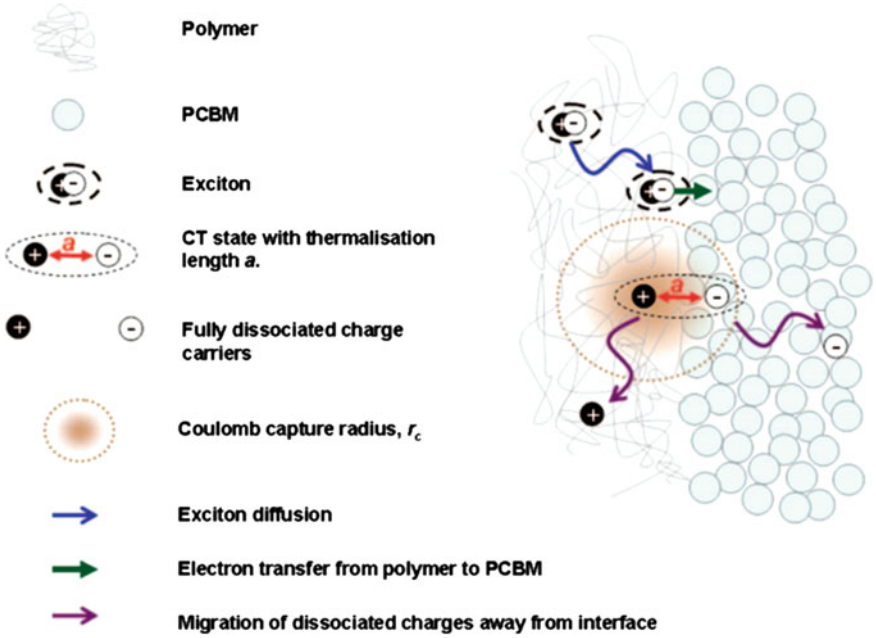

Fig. 9.2 Schematic of charge dissociation at the polymer:PCBM interface. Reproduced with permission from [28] Copyright 2010 American Chemical Society

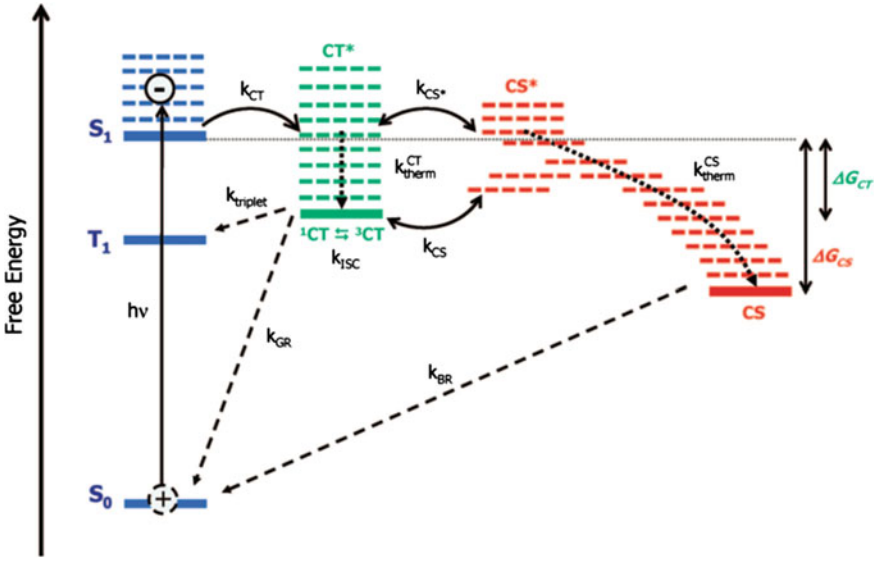

Fig. 9.3 Energy level diagram showing the charge photogeneration at donor/acceptor interface. Reproduced with permission from [28] Copyright 2010 American Chemical Society

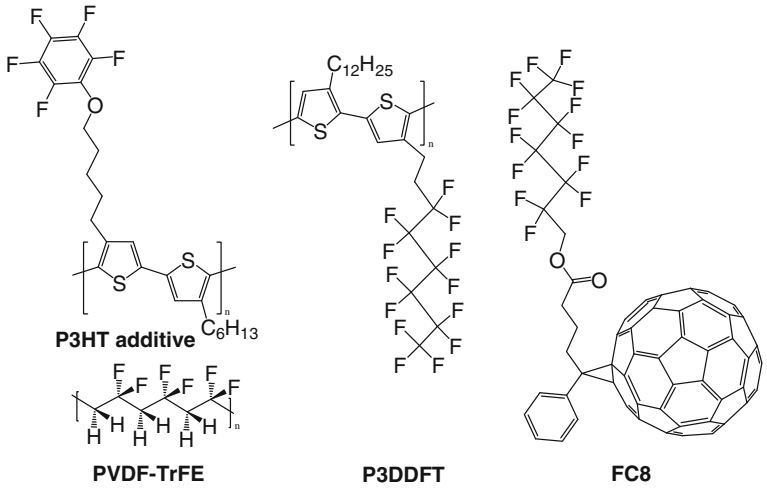

Fig. 9.4 Structure of dipole materials used as interfacial modifier at donor/acceptor junction

may result from bimolecular recombination (K_{BR}). The competition between charge separation and recombination is strongly influence the efficiency of charge photogeneration in organic solar cells [29]. Energy level offset and interfacial coupling at donor/acceptor interface are the important factors to influence charge photo generation. These electronic structures at interface depend on how the materials make contact, which in turn is governed by many factors such as interfacial dipole.

Recently, several studies demonstrated that proper treatment of polymer/fullerene interface in OPVs can influence their performance. Hashimoto et al. demonstrated a model of p–n junction PV build through connection of P3HT and PCBM layers by film-transfer method. Each semiconducting layer can be modified with a surface-segregated fluorinated PC8 (for PCBM) or P3DDFT (for P3HT) monolayer, which is reported to tune the strength and surface dipole direction. In their bilayer devices, introduction of interfacial dipole layer alter the device Voc with a wide range between 0.3 and 0.86 V. Authors attribute the effect to aligned dipole shift energy difference between the LUMO of the acceptor and the HOMO of the donor (ΔE_{HL} in Fig. 9.5). In case that FC8 on top of PCBM, interfacial dipole point from P3HT to PCBM, which downshift of ΔE_{HL}, to give a low Voc, 0.5 V. When planting P3DDFT on the top of P3HT, the interfacial dipole is reversed by pointing from PCBM to P3HT, thus enlarge ΔE_{HL} and Voc, 0.85 V [30].

Another approach to tune energy offset of the donor/acceptor junction is achieved with introduction of ferroelectric P(VDF-TrFE) layers. Recently, Huang et al. demonstrated that P3HT/PCBM bilayer devices with ultrathin P(VDF-TrFE) dipole layer at donor/acceptor interface to enlarge device Voc. As shown in Table 9.1. The Voc was increased from 0.55 to 0.67 V after poling the P(VDF-TrFE) layer with reverse bias on the device. Jsc and Voc showed increase. It is explained that dipole layer tune the relative energy level alignment at donor/acceptor junction. Both Jsc

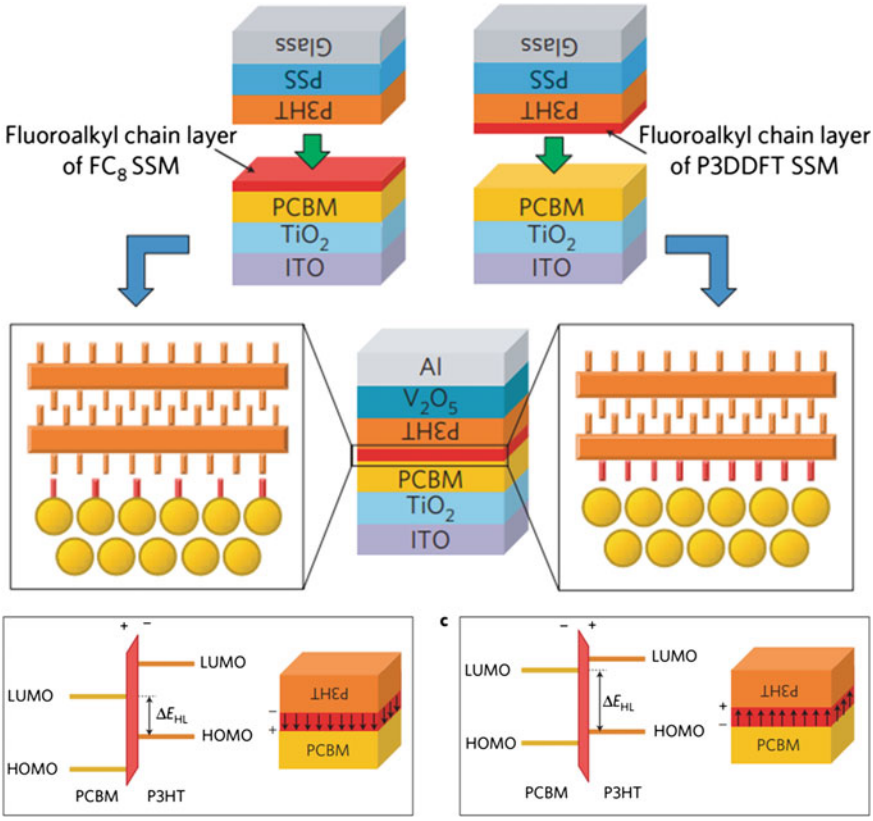

Fig. 9.5 Schematic representation and energy diagrams of the P3HT/PCBM bilayer devices with interfacial dipole layer of FC_8 and P3DDFT. Reproduced with permission from [30] Copyright 2010 Nature Publishing Group

and FF also increased due to the reduced recombination loss of charge-transfer excitons (CTEs) [31]. The dipoles of ferroelectric P(VDF-TrFE) can preserve their alignment after removing the polling field. The PCE is almost doubled with the polled dipole layer (P(VDF-TrFE). In the authors previous study, an ultrathin (1 nm) layer of P(VDF-TrFE) has been inserted between different BHJs and Al cathode to show significantly improved device characteristics [27].

It is interesting to see how the properties of organic/organic interfaces influence performance under conditions that more resemble those of an actual device. The ferroelectric PVDF-TrFE has been doped into bulk, which leads to better device performance from P3HT:PCBM BHJs [32]. The internal electric field enhancement estimate to be $\sim$150 and $\sim$300 V-m^{-1} for the devices with 5 and 10 % PVDF-TrFE concentration, which facilities singlet-exciton (SE) and charge-transfer-exciton (CTE) harvesting in BHJ, thus lead to IQE of BHJ devices approached 100 % for some wavelengths. Swager et al. reported that some fine-designed polymer

Table 9.1 Summary of device characteristics of representative polymer solar cells employing donor/acceptor interfacial engineering

Anode configuration	Active layer	Cathode configuration	V_{oc} (V)	J_{sc} (mA/cm^2)	FF	PCE (%)	References
ITO/TiO_2	$PC_{61}BM$/P3HT	V_2O_5/Al	0.50	1.51	0.53	0.40	[30]
ITO/TiO_2	$PC_{61}BM$/FC_8/P3HT	V_2O_5/Al	0.31	1.51	0.50	0.23	[30]
ITO/TiO_2	$PC_{61}BM$/P3DDFT/P3HT	V_2O_5/Al	0.86	0.70	0.38	0.23	[30]
ITO/PEDOT:PSS	P3HT/$PC_{61}BM$	Ca/Al	0.55	8.2	0.33	1.5	[31]
ITO/PEDOT:PSS	P3HT/PVDF-TrFE/$PC_{61}BM$	Ca/Al	0.67	9.0	0.55	3.3	[31]
ITO/PEDOT:PSS	P3HT:$PC_{61}BM$ (0 % PVDF-TrFE)	Al	0.55	9.6	0.48	2.5	[32]
ITO/PEDOT:PSS	P3HT:$PC_{61}BM$ (10 % PVDF-TrFE)	Al	0.57	11.3	0.60	3.9	[32]
ITO/PEDOT:PSS	P3HT:$PC_{61}BM$ (0.25 wt% additive)	Al	0.60	12.2	0.53	5.3	[33]

additives processing same polymer backbone with P3HT, while different polar side chain. The polymer additive (Fig. 9.4) was doped into P3HT/PCBM BHJ and proposed to be selectively localized at the donor/acceptor interface [33]. Authors suggested that polar aromatic moieties at side-chain termini at polymer/fullerene interface, decreasing the rate of bimolecular recombination and improves charge collection across the active layer. At low loadings of 0.25 % additive, the short circuit current and the series resistance have been optimized and yield ~30 % increase in PCE, which is up to 5.3 %.

Besides of aforementioned dipole (or polar) material modified donor/acceptor interface, strategies reported on selectively locating thiophene-fullerene dyads at the donor/acceptor interfaces were also interesting, since these approaches not only allow reducing the interfacial energy between immiscible components to stabilize the phase morphology, but also can serve as effective method to load materials at donor/acceptor interface. As shown in Fig. 9.6, Fréchet et al. demonstrated an amphiphilic di-block copolymer **1** could be used as an additive, also as a compatibilizer, to stabilize device structure against destructive thermal phase segregation

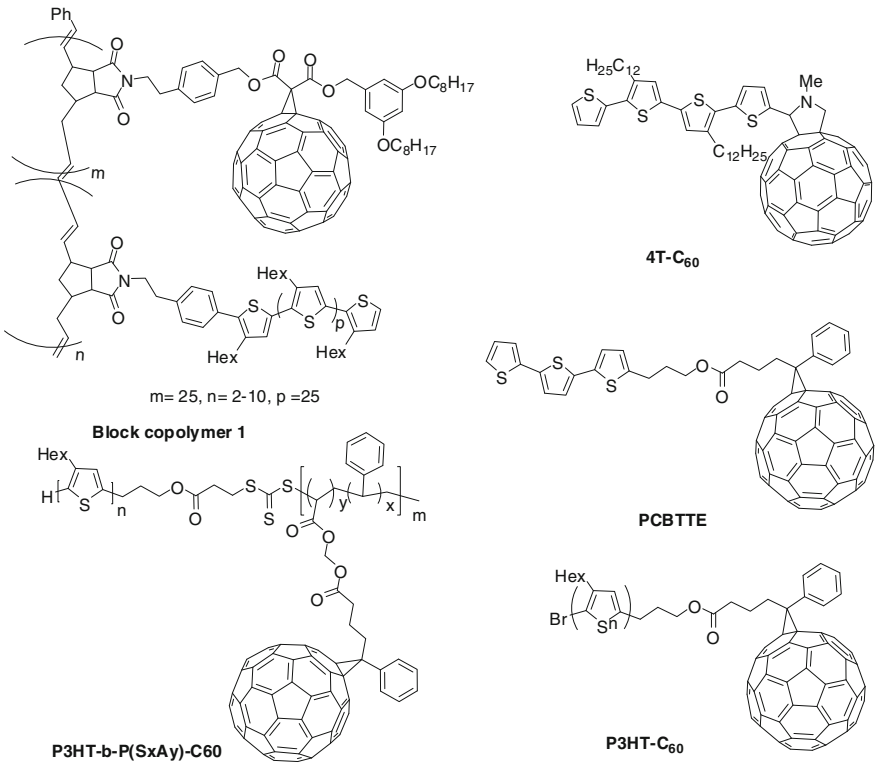

Fig. 9.6 Structure of thiophene-incorporated fullerene used as Morphology Stabilizer in BHJ

[34]. Another example was given using a well-defined rod–coil block copolymers (P3HT-b-P(SxAy)-C_{60}) [35]. Alternatively, A poly(3-hexylthiophene) end capped with fullerene (P3HT-C_{60}) [36] also exhibited effective control of BHJ morphology. In addition to block-copolymers, small thiophene-C_{60} derivatives [37, 38], such as 4T-C_{60} have been prepared by Loo et al. It showed a surface energy of 18.40 mN/m (4T-C_{60}), which is between that of P3HT (16.8 mN/m) and PCBM (30.1 mN/m). The addition of 4T-C_{60} reduces the interfacial energy between P3HT and PCBM, as evidenced by the constancy of the efficiency with thermal annealing at 170 for 3 h [39]. It effectively stabilized the blends (5 wt% to P3HT and PCBM) for PSC application.

9.1.2 Organic/Electrode Interface

In addition to the emerging studies on donor/acceptor interface engineering, most efforts related to interfacial engineering have been demonstrated on the improving organic/electrode contact. The introduction of proper interfacial materials have been proven to effectively optimize the electronic and electrical properties between the interfaces of active layer and electrode, which has become an important criterion to improve the performance of polymer solar cells. As reviewed by others [19–24] and ours [40–42], efficient interfacial materials for organic/electrode contact of OPV should generally fulfill several requirements, like (i) promote Ohmic contact formation between electrodes and the active layer; (ii) have appropriate energy levels to improve charge selectivity for corresponding electrodes; (iii) have large bandgap to confine excitons in the active layer; (iv) possess sufficient conductivity to reduce resistive losses, (v) have low absorption in the Vis-NIR wavelengths to minimize optical losses; (vi) have chemical and physical stability to prevent undesirable reactions at the active layer/electrode interface; (vii) have the ability to be processed from solution and at low temperatures; (viii) be mechanically robust to support multilayer solution processing; (ix) have good film forming properties and (x) be producible at low cost.

Several classes of materials and their hybrids had been introduced including conducting polymers, metal oxides, cross linkable materials, conjugated polymer electrolytes, self-assembled functional molecules and graphene-based materials. In this section, we mainly focus on discussing some of recent advancements on the design and application of interfacial materials in high-efficiency device. The chemical structures and energy diagram of some of the conjugated polymer donors and fullerene acceptors that will be discussed are shown in Figs. 9.7 and 9.8.

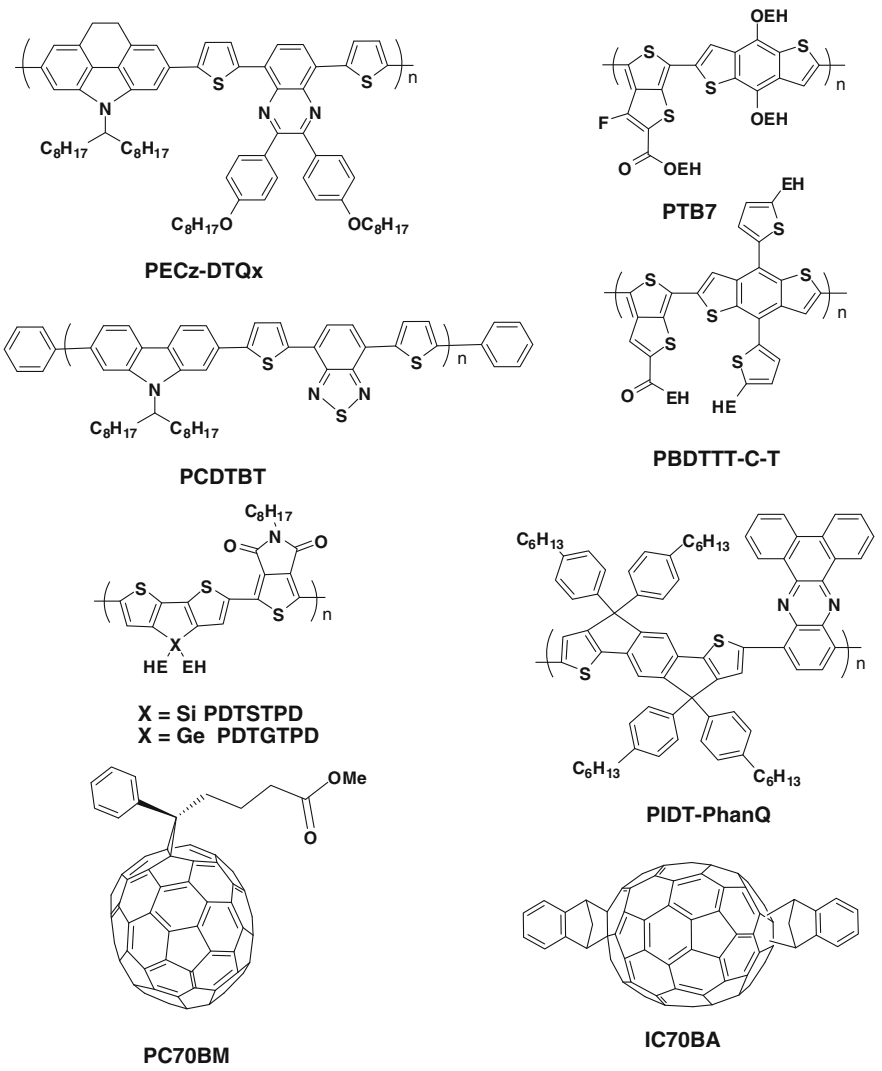

Fig. 9.7 Molecular structures of selected conjugated polymer donors and fullerene acceptors used as active materials in BHJs

9.2 Organic/Electrode Interfacial Materials for Conventional OPVs

The device characteristics of high-efficiency conventional OPVs employing newly developed interfacial layers are summarized in Table 9.2. PEDOT:PSS is the most commonly used solution-processible hole-transporting layer for anode modification

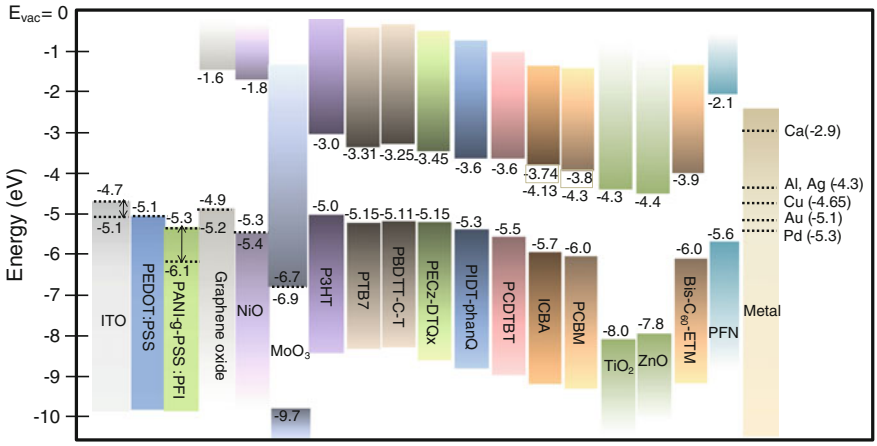

Fig. 9.8 Schematic view of the energy gaps and energy levels of some of the components of recent OPVs including transparent electrodes, hole selective materials, polymer donors, fullerene acceptors, electron selective materials and metal electrodes. The *dotted line* corresponds to the work functions of the materials. Adapted with permission from [42] Copyright 2012 Royal Society of Chemistry

in conventional solar cells. Some of the best reported OPV efficiencies are those using PEDOT:PSS as the hole-transporting layer [43, 44]. It has a wide range of electrical conductivities from 10^{-6} to 10^{3} S/cm (tuned by changing the compositional ratio between PEDOT+ and PSS− and processing with additives), work function ($\sim$5.1 eV) and optical transparency, which provide great flexibility in tuning the electrical property at the active layer/electrode interface. However, the deficiencies (strong acidity and hygroscopic nature) of PEDOT:PSS can induce chemical instability between the active layer and electrodes [45]. Some of the newly developed conducting polymers, PSSA-g-PANI [46] and sulfonated poly(diphenylamine) (SPDPA) [47] have been explored with tuned conductivity and acidity. Cross linkable materials were other classes of charge-transporting materials, and their crosslinked film improved solvent resistance for subsequent processing of the BHJ layer [48–51]. These new organic and polymeric hole-transporting materials exhibited the promise to replace PEDOT:PSS, but continuous improvement are still needed.

Besides of organic material, p-type inorganic transition metal oxides such as vanadium oxides (V_2O_5) [52] and nickel oxides (NiO) [53] have also been used as hole-selecting materials for OPVs, owning to their optical transparency and suitable energy level. Their conduction band is sufficiently higher than the LUMO of both organic donor and acceptor materials, for electron blocking. Work functions of p-type metal oxides (NiO $\sim$5.3 and V_2O_5 $\sim$5.3–5.4 eV) also can promote good Ohmic contact at the BHJ/anode interface with minimal contact resistance. As a result, good diode characteristics and fill factors of $\sim$70 % could be achieved in OPVs using optimized p-type NiO layers which outperform over PEDOT:PSS

Table 9.2 Summary of device characteristics of representative conventional polymer solar cells employing different interfacial layers

Anode configuration	Active layer	Cathode configuration	V_{oc} (V)	J_{sc} (mA/cm^2)	FF	PCE (%)	References
ITO/PEDOT:PSS	P3HT:$PC_{61}BM$	Ca/Al	0.61	10.6	0.67	4.4	[52]
ITO/NiO(sputtered)	P3HT:$PC_{61}BM$	LiF/Al	0.64	11.3	0.69	5.2	[53]
ITO/NiO_x (sol-gel)	PCDTBT:$PC_{71}BM$	Ca/Al	0.88	11.5	0.65	6.7	[54]
ITO/MoO_3(vac)	PCDTBT:$PC_{71}BM$	TiO_x(sol-gel)/Al	0.89	10.9	0.67	6.5	[63]
ITO/MoO_3(NPs)	P3HT:$PC_{61}BM$	Al	0.57	7.7	0.67	2.9	[67]
ITO/Graphene oxide	P3HT:$PC_{61}BM$	Al	0.57	11.4	0.54	3.5	[69]
ITO/PEDOT:PSS	P3HT:$PC_{61}BM$	TiO_x(sol-gel)Al	0.61	11.1	0.66	5.0	[75]
ITO/PEDOT:PSS	PCDTBT:$PC_{71}BM$	$TiO_{x(}$(sol-gel)/Al	0.88	10.6	0.66	6.1	[76]
ITO/PEDOT:PSS	P3HT:$PC_{61}BM$	TiO_2:Cs NPs/Al	0.58	10.8	0.67	4.2	[78]
ITO/PEDOT:PSS	P3HT:$PC_{61}BM$	ZnO NPs/SAM/Al (Ag, Au)	0.65	11.1	0.63	4.6	[80]
ITO/PEDOT:PSS	P3HT:$PC_{61}BM$	ZnO NPs-PEG/Al (Ag, Au)	0.60	10.7	0.69	4.4	[82]
ITO/PEDOT:PSS	P3HT:$PC_{61}BM$	P(VDF-TrFE)/Al	0.59	12.8	0.60	4.5	[27]
ITO/PEDOT:PSS	P3HT:$PC_{61}BM$	WPF-6-oxy-F/Al(Cu, Ag, Au)	0.64	10.1	0.60	3.9	[87]
ITO/PEDOT:PSS	PCDTBT:$PC_{71}BM$	PF2/6-*b*-P3TMAHT/Al	0.89	10.6	0.67	6.5	[84]
ITO/PEDOT:PSS	PECz-DTQx-$PC_{71}BM$	PFN/Al	0.81	11.4	0.66	6.1	[86]
ITO/PEDOT:PSS	PTB7:$PC_{71}BM$	PFN/Ca/Al	0.76	15.8	0.70	8.4	[88]
ITO/PEDOT:PSS	P3HT:$PC_{61}BM$	PEG-C_{60}/Al (Cu, Au)	0.66	10.5	0.65	4.4	[91]
ITO/PEDOT:PSS	PIDT-PhanQ:$PC_{71}BM$	C_{60}-surfactant/Ag (Al, Cu)	0.88	11.5	0.61	6.2	[93]

devices [53]. Recently, more promising approach form solution-processed NiO_x films is reported, which showed high PCE (6.7%) from PCDTBT:$PC_{71}BM$ BHJ and better stability than those PEDOT:PSS-based devices [54, 55]. A sol-gel derived VO_x film obtained by annealing at lower temperature (110 °C) also showed quite encouraging performance that is comparable to that of PEDOT:PSS-based devices but with better stability [56]. However, the optical absorption of VO_x in the visible range (400–500 nm) may limit its application as an efficient HSL.

Molybdenum oxides (MoO_3) and tungsten oxides (WO_3) have also been extensively investigated for anode modification in OPVs [52, 57, 58]. Its intrinsic n-type with deep-lying electronic states promote interfacial p-doping of various polymers [59], small molecules [60], and even fullerenes [61], since interfacial electron transfer from the organic semiconductor to MoO_3 is thermodynamically favorable. For example, the measured electron affinity, work function and ionization potentials for vacuum-deposited MoO_3 are −6.7, −6.86 and −9.68 eV [62]. The interfacial stability of OPVs based on evaporated MoO_3 film has been studied in different BHJ systems (P3HT:$PC_{61}BM$ and PCDTBT:$PC_{71}BM$) and the results showed that greatly enhanced lifetime could be achieved compared to the PEDOT:PSS-based devices [63, 64]. The recent demonstration of MoO_3 interfacial layers in OPV devices using either sol-gel processes [58, 65, 66] or nanoparticle suspensions [67, 68] further showed the promise of using metal oxides for anode modification.

Solution-processible Graphene Oxide (GO) is another promising HSL for OPVs [69]. Its HOMO and LUMO were measured to be −5.2 and −1.6 eV, which is good for hole transport and electron blocking, respectively. The work function of GO was between −4.9 and −5.1 eV, by scanning Kelvin probe microscopy [70]. Li et al. first explored the use of GO as HSL and reported that 2 nm GO nanosheets HSL in P3HT:PCBM OPV have comparable performance to that of PEDOT:PSS-based devices [69]. Further transient open-circuit voltage delay (TOCVD) measurements suggested that GO is more effective in suppressing leakage current and separating carriers via efficient hole-transporting to ITO and blocking of electrons. To further improve the anode contact, a hybrid bilayer structure based on GO and sol-gel processed NiO_x was developed [71], showing GO/NiO_x structure lead to major improvement of FF. These encouraging findings have opened the way for developing new interfacial materials for OPV.

Interface engineering for cathode is also very important for improving the performance of OPVs. In conventional OPVs, low work function cathode, such as Ca and Al are vulnerable to air and ambient condition. To improve the contact, vacuum-deposited materials such as BCP [72], PCBM [73], and C_{60}:LiF [74] have been introduced between the BHJ layer and the Al cathode. However, the development of solution processible ESLs is important for printable OPVs. The optimized ESLs should support the use of more stable and printable metals (such as colloidal Ag) as cathode for roll-to-roll manufacturing of OPV.

N-type metal oxides like TiO_2 and ZnO are the most widely studied ESL for OPVs. Using low temperature sol-gel processing, amorphous TiO_x films can be directly deposited on a BHJ layer to fabricate OPV devices [75]. The TiO_x films not only showed good electron selectivity, but also functioned as an optical spacer and

a good water and oxygen barrier, leading to significantly improved device efficiency and stability. The optical spacer effect of TiO_x has also been investigated in different BHJ systems. A PCE of 6.1 % has been reported when TiO_x interfacial layer was applied to a PCDTBT:$PC_{71}BM$ BHJ solar cell [76]. Furthermore, by replacing the anode PEDOT:PSS layer with MoO_3, the PCE of a PCDTBT:$PC_{71}BM$ device increased to 6.5 % and the stability of the device also improved significantly [63]. TiO_2 films prepared from solution processed crystalline nanoparticles (NPs) can also be used as an efficient ESL for OPVs [77]. By doping TiO_2 NP with Cs, it can further decrease the work function for more efficient electron extraction. As a result, the P3HT/PCBM based solar cells showed enhancements in PCE compared to those using a pure TiO_2 ESL [78]. ZnO is another efficient n-type metal oxide used for cathode modification in OPVs. Solution processed ZnO NP films has a high electron mobility (2.5 cm^2/Vs) [79], which can minimize Ohmic loss in the device. The electrical and electronic properties of ZnO can also be easily tuned by modifying the ZnO surface with a self-assembled molecular layer, to engineer the contact and surface dipoles between ZnO and metal, devices showed significant improvement in efficiency and it also enabled high work function metals such as Ag and Au to be used as cathode [80, 81]. Hybridization of ZnO NPs with poly(ethylene glycol) can also tune work function, morphology, refractive index and charge transporting properties of the ESL, which provides an efficient way to improve OPV performance [82]. The use of PVP as an organic capping molecule and polymeric matrix for ZnO modification produced electron-transporting nanocomposite films, which had excellent film-forming characteristics. Further UV-ozone treatment to remove PVP from the surface of the hybrid film consequently exposed the ZnO nanoclusters, which gave certificated PCE of 7.4 % from PDTG-TPD:PC71BM BHJ [83].

Organic-based interfacial materials that can be processed through orthogonal solvents of the BHJ layer were extensively studied ESL materials for OPVs. Their chemical structures are highlighted in Fig. 9.9. Conjugated polymers and polymer electrolytes that can be processed from alcoholic/water solvents attracted significant research attention in the past two years [84–86]. Polythiophene and polyfluorene with polar amines, amine salts, phosphates, and alkoxy side chains are the most commonly investigated systems. Oh et al. have demonstrated that an ESL based on a water soluble polyfluorene derivative (WPF-oxy-F) can effectively reduce the work functions of different metals including Al, Ag, Cu and Au, resulting in Ohmic contact between the P3HT:$PC_{61}BM$ BHJ and cathode to improve V_{oc} and PCE of the OPV [87]. Seo et al. demonstrated the effect of cationic polythiophene (P3TMAHT) and its polyfluorene block copolymer derivative (PF2/6-b-P3TMAHT) on PCDTBT:$PC_{71}BM$ based devices with improved PCE from 5 % to over 6.3 % [84].

Water/alcohol soluble polyfluorene derivative, PFN, which contains side chains terminated with neutral alkylamines has also been studied with BHJs composed of different polymer donors [88]. It was found that the improvements of PCE are relied heavily on the chemical structures of the polymer donors. Though the effect of PFN on P3HT and PPV-based OPVs was minimal, significant improvement of the PCE in a group of N-heterocycle-containing polymer donors was effectively

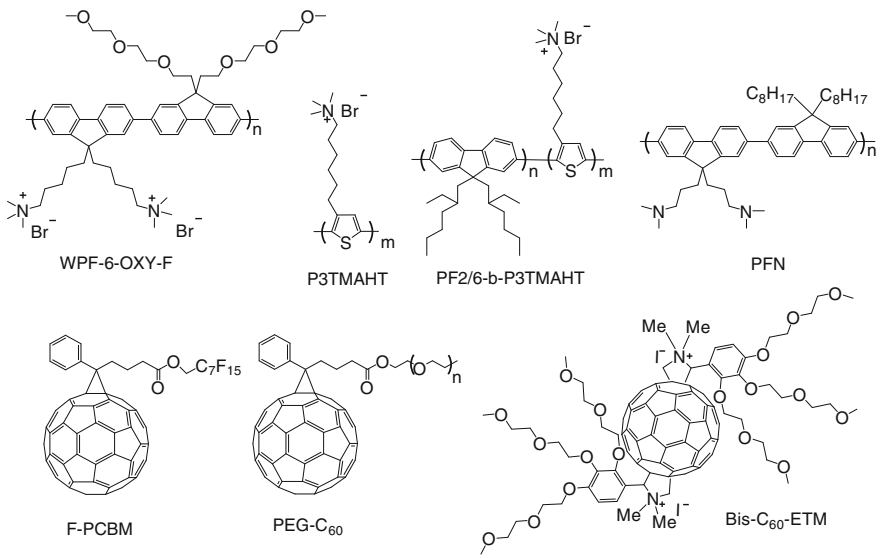

Fig. 9.9 Molecular structures of some electron selective materials used in conventional OPVs including conjugated polymer electrolytes and fullerene-based interfacial materials

demonstrated [89]. For example, OPVs based on PECz-DTQx:$PC_{71}BM$ showed PCE increases from 4.0 to 6.1 % when Al was used as cathode [85], while for the PCDTBT:$PC_{71}BM$ BHJ, the best device employed the PFN ESL in combination with a Ca/Al cathode, showing a PCE of 6.8 %. When high performance low bandgap polymer, PTB7 applied, a record OPV device performances with a PCE of 8.4 % were reported from PFN ESL modified Ca/Al cathode [86]. The authors suggested that the improved device performance could have multiple origins including enhanced built-in potential across the device, improved charge-transport, reduced space charge buildup, and minimized recombination losses due to increases in built-in field and charge carrier mobility.

Fullerene-based interfacial materials present another obvious option for ESL in BHJ OPVs since their energy levels, electron transport, and chemical compatibility to the BHJ fit the requirements of a good ESL. However, there are only limited reports of fullerene-based ESL, which is probably due to challenge in synthesizing proper fullerene materials with adequate solubility that can be used for solution processing. PCBM derivatives with fluorinated alkyl (F-PCBM) [90] and polymer (ethylene glycol) (PEG-C_{60}) [91, 92] are two interesting fullerene derivatives that have been explored as ESL. In both cases, small amounts of the fullerene derivatives were added into the P3HT:PCBM solution. During the film drying process, a thin layer of the fullerene derivative was found to segregate on the surface of the BHJ film, forming a self-organized interfacial layer. The OPV devices were then completed by evaporation of an Al cathode. In both cases, the fullerene surfactants were found to interact with the Al electrode, forming an appropriate interfacial

dipole that promoted better Ohmic contact and improved the device performance. Although the simplicity of self-organized ESLs is very attractive, it may not be generally applicable to different BHJ systems since the film drying kinetics may vary in different polymer:fullerene blends.

Fullerene ESLs that can be directly processed on top of different BHJ layers might represent a better option. This has been recently realized in a new fullerene derivative (bis-C_{60}-ETM) in which side chains composed of an amine salt and an alkoxy dendron were introduced to improve its solubility in alcohols [93, 94]. The bis-C_{60}-ETM could be directly spin-coated on top of the active layer to form a smooth ESL. To evaluate the general applicability of the fullerene ESL, devices based on different BHJs were tested and in all cases, the devices with bis-C_{60}-ETM showed significantly improved V_{oc}, J_{sc}, FF, and PCE. The effect of different metal cathodes (Al, Ag, and Cu) on the OPV efficiency and stability were further investigated based on the PIDT-phanQ:$PC_{71}BM$ BHJ system. The best PCE (6.6 %) was found when Ag was used as the cathode. Work function studies suggested that the bis-C_{60}-ETM film efficiently reduced the effective work functions of all three metals, which facilitated Ohmic contact at the BHJ/cathode interface to achieve a maximized V_{oc} independent of the choice of metal. However, devices with Cu and Ag cathodes showed much better ambient stability than the one with Al. These findings can be very important for developing efficient, stable, and roll-to-roll processible polymer solar cells.

9.3 Interfacial Materials for Inverted Structure OPVs

Since their initial application in 2006, inverted OPVs have attracted growing attention due to their improved stability and compatibility with roll-to-roll processes [95–97]. For inverted OPVs, the device polarity is reversed compared to that based on the conventional structure. The performance of the inverted OPV is critically dependent on the choice of the interfacial layers and their contact properties with the BHJ layer and the corresponding electrodes. The device characteristics of the representative inverted OPVs containing different interfacial layers and BHJ layers are summarized in Table 9.3.

Alkali metal salts can be used as an interfacial modifier to tune the work function of ITO for electron collection [98]. By spin-casting Cs_2CO_3 for ITO modification and V_2O_5 as the HSL underneath the Al top electrode, the PCE of inverted P3HT:PCBM BHJ OPVs could reach as high as 4.2 % [99]. It was found that upon annealing at 150 °C, Cs_2CO_3 will decompose to into doped cesium oxide (Cs_2O). This significantly improved electron collection by reducing the work function of ITO from 4.7 to 3.06 eV [100]. However, the insulating property of Cs_2O may limit its broader application for OPVs. TiO_2 and ZnO are the most widely studied electron selective materials for inverted OPVs. White et al. have demonstrated one of the earliest inverted P3HT:PCBM BHJ solar cells based on a sol-gel derived ZnO film on ITO as the ESL and an Ag anode as the top electrode [101].

Table 9.3 Summary of device characteristics of representative inverted polymer solar cells employing different interfacial layers

Cathode configuration	Active layer	Anode configuration	V_{oc} (V)	J_{sc} (mA/cm^2)	FF	PCE (%)	References
ITO/Cs_2CO_3	P3HT:$PC_{61}BM$	V_2O_5/Al	0.59	11.1	0.63	4.2	[99]
ITO/TiO_x(sol-gel)	P3HT:$PC_{61}BM$	PEODT:PSS/Au	0.56	9.0	0.62	3.1	[126]
ITO/TiO_x/FPQ-Br	P3HT:$PC_{61}BM$	MoO_3/Au	0.58	8.9	0.70	3.6	[127]
ITO/TIPD	PBDTTT-C-T:$PC_{71}BM$	MoO3/Ag	0.70	16.26	0.65	7.4	[114]
ITO/WPF-6-oxy-F	P3HT:$PC_{61}BM$	PEDOT:PSS/Ag	0.66	8.8	0.59	3.4	[128]
ITO/ZnO(sol-gel)	PDTGTPD:$PC_{71}BM$	MoO_3/Ag	0.85	12.6	0.68	7.3	[103]
ITO/ZnO(sol-gel)	PCDTBT:$PC_{71}BM$	MoO_3/Ag	0.88	10.4	0.69	6.3	[129]
ITO/ZnO(sol-gel)	aPTPTBT:$PC_{71}BM$	VO_x (sol-gel)/Ag	0.82	11.6	0.53	5.0	[104]
ITO/ZnO NPs	P3HT:$PC_{61}BM$	PEDOT:PSS/Ag	0.62	10.7	0.54	3.6	[107]
ITO/ZnO NPs/C_{60}-SAM	P3HT:$PC_{61}BM$	PEDOT:PSS/Ag	0.63	12.0	0.61	4.5	[107]
ITO/ZnO(sol-gel)/C-PCBSD	P3HT:$PC_{61}BM$	PEDOT:PSS/Ag	0.60	12.8	0.58	4.4	[109]
ITO/ZnO(sol-gel)/C-PCBSD	P3HT:ICBA	PEDOT:PSS/Ag	0.84	12.4	0.60	6.2	[110]
ITO/ZnO–PVP	PDTGTPD:$PC_{71}BM$	MoO_3/Ag	0.86	14.0	0.67	8.1	[83]
ITO/PEIE	P3HT:ICBA	MoO_3/Ag	0.81	11	0.66	5.9	[112]
ITO/BPCO	PCDTBT:PC71BM	MoO_3/Ag	0.89	9.5	0.62	6.2	[113]
ITO/n-doped P-PCBM-S	P3HT:$PC_{61}BM$	PEDOT:PSS/Ag	0.63	9.1	0.44	2.5	[115]
ITO/n-doped PNDI-1Th	P3HT:$PC_{61}BM$	PEDOT:PSS/Ag	0.59	10.0	0.58	3.4	[116]
ITO/ZnO NPs/C_{60}-SAM	P3HT:$PC_{61}BM$	GO/Ag (Au,Al)	0.62	10.3	0.62	3.9	[122]
ITO/ZnO NPs	PIDT-phanQ:$PC_{71}BM$	GO/Ag	0.86	10.9	0.62	5.9	[125]

The crystallinity of the ZnO films could be increased by thermal annealing at 300 °C to improve their electrical properties. By inserting a thermally evaporated HSL, such as V_2O_5 or MoO_3 between the BHJ layer and metal anode, it promotes better Ohmic contact at the anode, leading to further improved ZnO-based inverted OPVs [102]. Such a device platform has shown good compatibility with different BHJ layers. Recently, very high efficiency inverted OPVs were demonstrated based on PDTSTPD:$PC_{71}BM$ and PDTGTPD:$PC_{71}BM$ BHJ layers with PCEs of 6.6 and 7.3 %, respectively [103].

In addition to the n-type metal oxides as ESL, the development of solution processed p-type metal oxide as HSL for inverted cells is equally important. Chen et al. have demonstrated that a VO_x HSL could be prepared by spin-coating the sol-gel solution on the BHJ layer followed by low temperature annealing at 100 °C [104]. Inverted P3HT:$PC_{61}BM$ and PTPBT:$PC_{71}BM$ devices showed enhanced performance as a result of increased Jsc. The encapsulated inverted devices also showed very good thermal stability with no performance loss after annealing at 65 °C for 1,000 h. These results are very encouraging since low temperature process is more compatible with flexible plastic substrates.

The modification of metal oxide films with functional SAMs can efficiently alter the interfacial properties between the ESL and BHJ. Bulliard et al. [105] reported that the morphology of the BHJ film could be optimized by virtue of a ZnO surface with tailored surface energy leading to an improved PCE in inverted cells. This can be achieved by changing the surface compositions of the two different SAMs with either polar $–NH_2$ or non-polar $–CH_3$ end groups, resulting in a wide range of surface energies from 40 to 70 mN/m. Modification of metal oxides with fullerene-based SAMs have also been employed to improve the ESL/BHJ contact. It was found that good quality fullerene-SAM (C_{60}-SAM) with proper anchor groups could be obtained by simple spin-coating on ZnO [106]. The C_{60}-SAM serves multiple purposes, including enhancement of interfacial exciton-dissociation efficiency, passivation of inorganic-surface trap states, and optimization of upper organic layer morphology. As a result, a C_{60}-SAM modified P3HT:PCBM inverted cell showed improved PCE from 3.7 to 4.5 % [107]. This strategy has also been applied to other BHJ layer composed of new low bandgap polymers, which resulted in similar improvement in device efficiency [108]. The interfacial property between the metal oxide ESL and the BHJ can also be improved by inserting a thin layer of crosslinked fullerenes(C-PCBSD) (Fig. 9.10) [109, 110]. In situ cross-linking of the PCBSD film on ZnO could be achieved by annealing the film at 160 °C for 30 min to generate a robust, adhesive, and solvent-resistant film, showing an improvement of the performance of inverted P3HT:PCBM OPV from 3.5 to 4.4 %, and inverted P3HT:ICBA from 4.8 to 6.2 % [111].

Compared to their inorganic counterparts, organic materials as ESL is less explored in spite of their promise as interfacial materials for OPVs. Organic materials allow tailoring to have versatile functionalities. Their intrinsic mechanical robustness and flexibility are more suitable for flexible OPVs. Recent studies from Kippelen et al. demonstrated water soluble polymer surfactant, PEIE (Fig. 9.10) can strongly modified ITO electrodes and greatly shift its work function more than

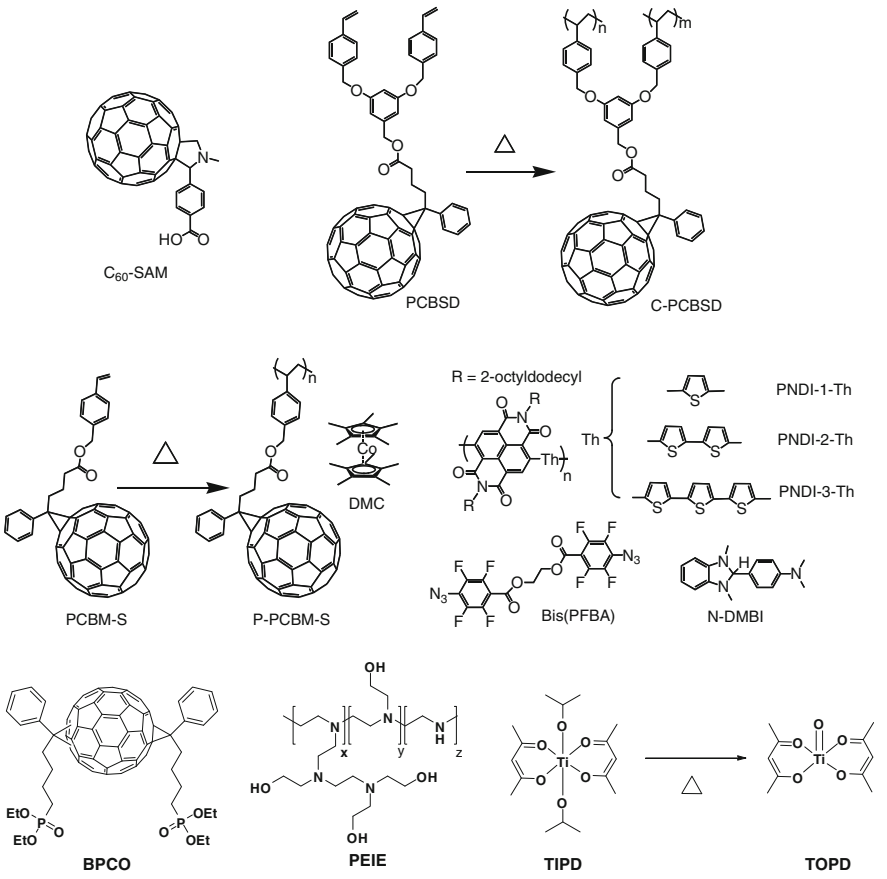

Fig. 9.10 Molecular structures of electron selective materials used in inverted OPV

1 eV. An ultrathin layer of insulating PEIE (<10 nm) on glass ITO can get PCE of 5.9 % from P3HT:ICBA BHJ, and all polymer based devices with a PEIE-coated PH1000 bottom electrode yielded high durability toward repeated bending [112]. A phosphate-containing bisadducts fullerene (B-PCPO) with alcohol solubility and good electron transporting ability also showed good application as ESL for inverted OPV, showed improvement of performance from 4.83 % (ITO) to 6.20 % (B-PCPO/ITO) [113]. Inverted PSCs based on PBDTTT-C/PC71BM with iso-propanol solution-processed TIPD as ESL on ITO was reported 7.4 % PCE, which was facilitated by thermal convert of TIPD to TOPD at 150 °C [114].

One of the major limitations of interfacial organic materials is their low inherent conductivities. To overcome this limitation, n-doping of organic-based ESL has been applied to improve the contact [115–117]. A n-doped polymerizable PCBM-S ESL provide not only good solvent resistance, but also improve conductivity from 1.7×10^{-7} S/m (undoped film) to 6.0×10^{-1} S/m (10 % decamethylcobaltocene

(DMC) doped film). N-doped ESL showed improved J-V characteristics and PCE [115]. Similar strategy was studied by using N-doped cross linkable ESL layer. An in situ n-doping and crosslinking of a series of naphthalene diimide and thiophene copolymers (NPDI-Th) has been studied with bis-PFPA crosslinker [118] and N-DMBI dopant [119] to generate conductive ESLs, resulted in significant increased electrical conductivity, as a result, the PCE of inverted P3HT:PCBM OPVs increased from 0.69 to 3.42 % [116].

For anode modification of inverted cells, besides the widely used PEDOT:PSS, n-type metal oxides such as WO_3 and MoO_3 are efficient materials that can promote Ohmic contact between the BHJ layer and metal anode due to their ability to p-dope the polymer donor [59, 120, 121]. GO as the HSL were also reported for anode modification of inverted OPVs [122–124]. Inverted P3HT:PCBM-based OPV devices modified with a 2–3 nm thick of GO HSL exhibited a remarkable improved PCE compared to devices without any interfacial layer and is even slightly better than that of PEDOT:PSS-based devices, indicating GO can effectively modify the anode to facilitate efficient hole collection [123]. It was found that protonic acid doping of the conjugated polymer at the BHJ/GO interface occurred due to the high proton density of GO, resulted in a highly conductive interface that facilitated Ohmic contact with the metal anode [122]. Another good example was recently demonstrated in inverted OPV based on PIDT-PhanQ:$PC_{71}BM$ BHJ, which showed a PCE of 5.9 % when GO was used as the HSL [125].

9.4 Conclusions

The introduction of proper interfacial materials to optimize properties between organic/metal and organic/organic interfaces has been turn out to be an equally important criterion as the design and process of new active materials, both of which pave the way to high performance and stability of organic photovoltaics. This chapter aimed to provide an overview on the recent development of effective interfacial materials, and the integration of these materials in different device architectures. Regarding to organic/electrode interface, tremendous progress have been achieved with developing several classes of organic, inorganic and hybrid interfacial materials, including conducting polymers, metal oxides, cross linkable materials, conjugated polymer electrolytes, self-assembled functional molecules and graphene-based materials. The electronic, electrical, optical, chemical and mechanical properties of interlayer materials are considered to be improved for maximizing PCE and device stability. For the emerging studies involved donor/acceptor interface engineering, it is critical to achieve in-depth understanding of physic at this organic/organic interface. The development of new strategies and materials to get control of the chemical and physical properties at these interfaces are very important for improving OPV technology.

Acknowledgments The authors thank the support from the National Science Foundation (DMR-0120967), the Department of Energy (DE-FC3608GO18024/A000), the Air Force Office of Scientific Research (FA9550-09-1-0426), the Asian Office of Aerospace R&D (FA2386-11-1-4072), Office of Naval Research (N00014-11-1-0300). A.K.-Y.J. thanks the Boeing Foundation for support.

References

1. http://www.eia.doe.gov/oiaf/ieo/index.html
2. C.J. Brabec, G. Dennler, M.C. Scharber, Adv. Mater. **21**, 1323 (2009)
3. F.C. Krebs, Sol. Energy Mater. Sol. Cells **93**, 394 (2009)
4. C.W. Tang, Appl. Phys. Lett. **48**, 183 (1986)
5. M.A. Green, K. Emery, Y. Hishikawa, W. Warta, E.D. Dunlop, Prog Photovoltaics **19**, 565 (2011)
6. R. F. Service, Science **332**, 293 (2011)
7. E. Bundgaard, F.C. Krebs, Sol. Energ. Mat. Sol. C **91**, 954 (2007)
8. Y.J. Cheng, S.H. Yang, C.S. Hsu, Chem. Rev. **109**, 5868 (2009)
9. Y. Liang, L. Yu, Acc. Chem. Res. **43**, 1227 (2010)
10. G. Li, V. Shrotriya, J. Huang, Y. Yao, T. Moriarty, K. Emery, Y. Yang, Nat. Mater. **4**, 864 (2005)
11. J. Peet, M.L. Senatore, A.J. Heeger, G.C. Bazan, Adv. Mater. **21**, 1521 (2009)
12. F.C. Krebs, Sol. Energ. Mat. Sol. C **93**, 394 (2009)
13. H. Ma, H.-L. Yip, F. Huang, A.K.Y. Jen, Adv. Funct. Mater. **20**, 1371 (2010)
14. L.-M. Chen, Z. Xu, Z. Hong, Y. Yang, J. Mater. Chem. **20**, 2575 (2010)
15. E.D. Gomez, Y.-L. Loo, J. Mater. Chem. **20**, 6604 (2010)
16. R. Steim, F.R. Kogler, C.J. Brabec, J. Mater. Chem. **20**, 2499 (2010)
17. J.H. Park, T.-W. Lee, B.-D. Chin, D.H. Wang, O.O. Park, Macromol. Rapid Comm. **31**, 2095 (2010)
18. R. Po, C. Carbonera, A. Bernardi, N. Camaioni, Energy Environ. Sci. **4**, 285 (2011)
19. S. Braun, W.R. Salaneck, M. Fahlman, Adv. Mater. **21**, 1450 (2009)
20. W.J. Potscavage Jr, A. Sharma, B. Kippelen, Acc. Chem. Res. **42**, 1758 (2009)
21. E.L. Ratcliff, B. Zacher, N.R. Armstrong, J. Phys. Chem. Lett. **2**, 1337 (2011)
22. C. Deibel, V. Dyakonov, Rep. Prog. Phys. **73**, 096401 (2010)
23. J. Hwang, A. Wan, A. Kahn, Mat. Sci. Eng. R **64**, 1 (2009)
24. P.W.M. Blom, V.D. Mihailetchi, L.J.A. Koster, D.E. Markov, Adv. Mater. **19**, 1551 (2007)
25. V.D. Mihailetchi, P.W.M. Blom, J.C. Hummelen, M.T. Rispens, J. Appl. Phys. **94**, 6849 (2003)
26. J.-L. Brédas, J.E. Norton, J. Cornil, V. Coropceanu, Acc. Chem. Res. **42**, 1691 (2009)
27. Y.B. Yuan, T.J. Reece, P. Sharma, S. Poddar, S. Ducharme, A. Gruverman, Y. Yang, J.S. Huang, Nat. Mater. **10**, 296 (2011)
28. T.M. Clarke, J.R. Durrant, Chem. Rev. **110**, 6736 (2010)
29. K. Tvingstedt, K. Vandewal, A. Gadisa, F. Zhang, J. Manca, O. Inganäs, J. Am. Chem. Soc. **131**, 11819 (2009)
30. A. Tada, Y. Geng, Q. Wei, K. Hashimoto, K. Tajima, Nat. Mater. **10**, 450 (2011)
31. B. Yang, Y. Yuan, P. Sharma, S. Poddar, R. Korlacki, S. Ducharme, A. Gruverman, R. Saraf, J. Huang, Adv. Mater. **24**, 1455 (2012)
32. K.S. Nalwa, J.A. Carr, R.C. Mahadevapuram, H.K. Kodali, S. Bose, Y. Chen, J.W. Petrich, B. Ganapathysubramanian, S. Chaudhary, Energ. Environ. Sci. **5**, 7042 (2012)
33. J.M. Lobez, T.L. Andrew, V. Bulović, T.M. Swager, ACS Nano **6**, 3044 (2012)
34. K. Sivula, Z.T. Ball, N. Watanabe, J.M.J. Fréchet, Adv. Mater. **18**, 206 (2006)
35. C. Yang, J.K. Lee, A.J. Heeger, F. Wudl, J. Mater. Chem. **19**, 5416 (2009)

36. M. Wang, A.J. Heeger, F. Wudl, Small **7**, 298 (2011)
37. T. Nishizawa, K. Tajima, K. Hashimoto, J. Mater. Chem. **17**, 2440 (2007)
38. J.L. Segura, N. Martin, D.M. Guldi, Chem. Soc. Rev. **34**, 31 (2005)
39. J.B. Kim, K. Allen, S.J. Oh, S. Lee, M.F. Toney, Y.S. Kim, C.R. Kagan, C. Nuckolls, Y.L. Loo, Chem. Mater. **22**, 5762 (2010)
40. H. Ma, H.-L. Yip, F. Huang, A.K.Y. Jen, Adv. Func. Mater. **20**, 1371 (2010)
41. C.-Z. Li, H.-L. Yip, A.K.Y. Jen, J. Mater. Chem. **22**, 4161 (2012)
42. H.-L. Yip, A.K.Y. Jen, Energy. Environ. Sci. **5**, 5994 (2012)
43. Y. Liang, Z. Xu, J. Xia, S.-T. Tsai, Y. Wu, G. Li, C. Ray, L. Yu, Adv. Mater. **22**, E135 (2010)
44. H.-Y. Chen, J. Hou, S. Zhang, Y. Liang, G. Yang, Y. Yang, L. Yu, Y. Wu, G. Li, Nat. Photonics **3**, 649 (2009)
45. K.W. Wong, H.L. Yip, Y. Luo, K.Y. Wong, W.M. Lau, K.H. Low, H.F. Chow, Z.Q. Gao, W.L. Yeung, C.C. Chang, Appl. Phys. Lett. **80**, 2788 (2002)
46. J.W. Jung, J.U. Lee, W.H. Jo, J. Phys. Chem. C **114**, 633 (2010)
47. C.-Y. Li, T.-C. Wen, T.-F. Guo, J. Mater. Chem. **18**, 4478 (2008)
48. A.W. Hains, T.J. Marks, Appl. Phys. Lett. **92**, 023504 (2008)
49. A.W. Hains, J. Liu, A.B.F. Martinson, M.D. Irwin, T.J. Marks, Adv. Funct. Mater. **20**, 595 (2010)
50. A.W. Hains, C. Ramanan, M.D. Irwin, J. Liu, M.R. Wasielewski, T.J. Marks, ACS Appl. Mater. Inter. **2**, 175 (2010)
51. Y. Sun, S.-C. Chien, H.-L. Yip, Y. Zhang, K.-S. Chen, D.F. Zeigler, F.-C. Chen, B. Lin, A. K.Y. Jen, Chem. Mater. **23**, 5006 (2011)
52. V. Shrotriya, G. Li, Y. Yao, C.W. Chu, Y. Yang, Appl. Phys. Lett. **88**, 073508 (2006)
53. M.D. Irwin, B. Buchholz, A.W. Hains, R.P.H. Chang, T.J. Marks, P. Natl. Acad. Sci. U.S.A. **105**, 2783 (2008)
54. K.X. Steirer, P.F. Ndione, N.E. Widjonarko, M.T. Lloyd, J. Meyer, E.L. Ratcliff, A. Kahn, N.R. Armstrong, C.J. Curtis, D.S. Ginley, J.J. Berry, D.C. Olson, Adv. Energy Mater. **1**, 813 (2011)
55. K.X. Steirer, J.P. Chesin, N.E. Widjonarko, J.J. Berry, A. Miedaner, D.S. Ginley, D.C. Olson, Org. Electron. **11**, 1414 (2010)
56. K. Zilberberg, S. Trost, H. Schmidt, T. Riedl, Adv. Energy Mater. **1**, 377 (2011)
57. S. Han, W.S. Shin, M. Seo, D. Gupta, S.-J. Moon, S. Yoo, Org. Electron. **10**, 791 (2009)
58. S. Murase, Y. Yang, Adv. Mater. **24**, 2459 (2012)
59. M.C. Gwinner, R. Di Pietro, Y. Vaynzof, K.J. Greenberg, P.K.H. Ho, R.H. Friend, H. Sirringhaus, Adv. Funct. Mater. **21**, 1432 (2011)
60. T. Matsushima, G.-H. Jin, Y. Kanai, T. Yokota, S. Kitada, T. Kishi, H. Murata, Org. Electron. **12**, 520 (2011)
61. M. Kubo, K. Iketaki, T. Kaji, M. Hiramoto, Appl. Phys. Lett. **98**, 073311 (2011)
62. M. Kroger, S. Hamwi, J. Meyer, T. Riedl, W. Kowalsky, A. Kahn, Appl. Phys. Lett. **95**, 123301 (2009)
63. Y. Sun, C.J. Takacs, S.R. Cowan, J.H. Seo, X. Gong, A. Roy, A.J. Heeger, Adv. Mater. **23**, 2226 (2011)
64. E. Voroshazi, B. Verreet, A. Buri, R. Mueller, D. Di Nuzzo, P. Heremans, Org. Electron. **12**, 736 (2011)
65. F. Liu, S. Shao, X. Guo, Y. Zhao, Z. Xie, Sol. Energ. Mat. Sol. C **94**, 842 (2010)
66. C. Girotto, E. Voroshazi, D. Cheyns, P. Heremans, B.P. Rand, ACS Appl. Mater. Inter. **3**, 3244 (2011)
67. T. Stubhan, T. Ameri, M. Salinas, J. Krantz, F. Machui, M. Halik, C.J. Brabec, Appl. Phys. Lett. **98**, 253308 (2011)
68. J. Meyer, R. Khalandovsky, P. Gorrn, A. Kahn, Adv. Mater. **23**, 70 (2011)
69. S.S. Li, K.H. Tu, C.C. Lin, C.W. Chen, M. Chhowalla, ACS Nano **4**, 3169 (2010)
70. K.-H. Tu, S.-S. Li, W.-C. Li, D.-Y. Wang, J.-R. Yang, C.-W. Chen, Energ. Environ. Sci. **4**, 3521 (2011)

71. M.S. Ryu, J. Jang, Sol. Energ. Mat. Sol. C **95**, 2893 (2011)
72. C.-C. Chang, C.-F. Lin, J.-M. Chiou, T.-H. Ho, Y. Tai, J.-H. Lee, Y.-F. Chen, J.-K. Wang, L.-C. Chen, K.-H. Chen, Appl. Phys. Lett. **96**, 263506 (2010)
73. A. Kumar, G. Li, Z. Hong, Y. Yang, Nanotechnology **20**, 165202 (2009)
74. D. Gao, M.G. Helander, Z.B. Wang, D.P. Puzzo, M.T. Greiner, Z.H. Lu, Adv. Mater. **22**, 5404 (2010)
75. J.Y. Kim, S.H. Kim, H.H. Lee, K. Lee, W.L. Ma, X. Gong, A.J. Heeger, Adv. Mater. **18**, 572 (2006)
76. S.H. Park, A. Roy, S. Beaupre, S. Cho, N. Coates, J.S. Moon, D. Moses, M. Leclerc, K. Lee, A.J. Heeger, Nat. Photonics **3**, 297 (2009)
77. T. Salim, Z. Yin, S. Sun, X. Huang, H. Zhang, Y.M. Lam, ACS Appl. Mater. Inter. **3**, 1063 (2011)
78. M.-H. Park, J.-H. Li, A. Kumar, G. Li, Y. Yang, Adv. Funct. Mater. **19**, 1241 (2009)
79. H. Faber, M. Burkhardt, A. Jedaa, D. Kaelblein, H. Klauk, M. Halik, Adv. Mater. **21**, 3099 (2009)
80. H.-L. Yip, S.K. Hau, N.S. Baek, A.K.Y. Jen, Appl. Phys. Lett. **92**, 193313 (2008)
81. H.-L. Yip, S.K. Hau, N.S. Baek, H. Ma, A.K.Y. Jen, Adv. Mater. **20**, 2376 (2008)
82. S.B. Jo, J.H. Lee, M. Sim, M. Kim, J.H. Park, Y.S. Choi, Y. Kim, S.-G. Ihn, K. Cho, Adv. Energy Mater. **1**, 690 (2011)
83. C.E. Small, S. Chen, J. Subbiah, C.M. Amb, S.-W. Tsang, T.-H. Lai, J.R. Reynolds, F. So, Nat. Photon **6**, 115 (2012)
84. J.H. Seo, A. Gutacker, Y. Sun, H. Wu, F. Huang, Y. Cao, U. Scherf, A.J. Heeger, G.C. Bazan, J. Am. Chem. Soc. **133**, 8416 (2011)
85. Z. He, C. Zhang, X. Xu, L. Zhang, L. Huang, J. Chen, H. Wu, Y. Cao, Adv. Mater. **23**, 3086 (2011)
86. Z. He, C. Zhong, X. Huang, W.-Y. Wong, H. Wu, L. Chen, S. Su, Y. Cao, Adv. Mater. **23**, 4636 (2011)
87. S.H. Oh, S.I. Na, J. Jo, B. Lim, D. Vak, D.Y. Kim, Adv. Funct. Mater. **2010**, 20 (1977)
88. C. He, C. Zhong, H. Wu, R. Yang, W. Yang, F. Huang, G.C. Bazan, Y. Cao, J. Mater. Chem. **20**, 2617 (2010)
89. L.J. Zhang, C. He, J.W. Chen, P. Yuan, L.A. Huang, C. Zhang, W.Z. Cai, Z.T. Liu, Y. Cao, Macromolecules **43**, 9771 (2010)
90. Q. Wei, T. Nishizawa, K. Tajima, K. Hashimoto, Adv. Mater. **20**, 2211 (2008)
91. J.W. Jung, J.W. Jo, W.H. Jo, Adv. Mater. **23**, 1782 (2011)
92. Q.D. Tai, J.H. Li, Z.K. Liu, Z.H. Sun, X.Z. Zhao, F. Yan, J. Mater. Chem. **21**, 6848 (2011)
93. K. O'Malley, C.-Z. Li, H.L. Yip, A.K. Y. Jen, under review
94. C.-Z. Li, C.-C. Chueh, H.-L. Yip, K.M. O'Malley, W.-C. Chen, A.K.Y. Jen, J. Mater. Chem. **22**, 8574 (2012)
95. L.-M. Chen, Z. Hong, G. Li, Y. Yang, Adv. Mater. **21**, 1434 (2009)
96. S.K. Hau, H.-L. Yip, A.K.Y. Jen, Polym. Rev. **50**, 474 (2010)
97. F. Zhang, X. Xu, W. Tang, J. Zhang, Z. Zhuo, J. Wang, J. Wang, Z. Xu, Y. Wang, Sol. Energ. Mat. Sol. C, **95**, 1785
98. M. Reinhard, J. Hanisch, Z. Zhang, E. Ahlswede, A. Colsmann, U. Lemmer, Appl. Phys. Lett. **98**, 053303 (2011)
99. H.H. Liao, L.M. Chen, Z. Xu, G. Li, Y. Yang, Appl. Phys. Lett. **92**, 173303 (2008)
100. J.S. Huang, G. Li, Y. Yang, Adv. Mater. **20**, 415 (2008)
101. M.S. White, D.C. Olson, S.E. Shaheen, N. Kopidakis, D.S. Ginley, Appl. Phys. Lett. **89**, 143517 (2006)
102. A.K.K. Kyaw, X.W. Sun, C.Y. Jiang, G.Q. Lo, D.W. Zhao, D.L. Kwong, Appl. Phys. Lett. **93**, 221107 (2008)
103. C.M. Amb, S. Chen, K.R. Graham, J. Subbiah, C.E. Small, F. So, J.R. Reynolds, J. Am. Chem. Soc. **133**, 10062 (2011)
104. C.-P. Chen, Y.-D. Chen, S.-C. Chuang, Adv. Mater. **23**, 3859 (2011)

105. X. Bulliard, S.-G. Ihn, S. Yun, Y. Kim, D. Choi, J.-Y. Choi, M. Kim, M. Sim, J.-H. Park, W. Choi, K. Cho, Adv. Funct. Mater. **20**, 4381 (2010)
106. S.K. Hau, Y.-J. Cheng, H.-L. Yip, Y. Zhang, H. Ma, A.K.Y. Jen, ACS Appl. Mater. Inter. **2010**, 2 (1892)
107. S.K. Hau, H.-L. Yip, H. Ma, A.K.Y. Jen, Appl. Phys. Lett. **93**, 233304 (2008)
108. Y. Zhang, S.K. Hau, H.-L. Yip, Y. Sun, O. Acton, A.K.Y. Jen, Chem. Mater. **22**, 2696 (2010)
109. C.-H. Hsieh, Y.-J. Cheng, P.-J. Li, C.-H. Chen, M. Dubosc, R.-M. Liang, C.-S. Hsu, J. Am. Chem. Soc. **132**, 4887 (2010)
110. Y.-J. Cheng, F.-Y. Cao, W.-C. Lin, C.-H. Chen, C.-H. Hsieh, Chem. Mater. **23**, 1512 (2011)
111. Y.-J. Cheng, C.-H. Hsieh, Y. He, C.-S. Hsu, Y. Li, J. Am. Chem. Soc. **132**, 17381 (2010)
112. Y. Zhou, C. Fuentes-Hernandez, J. Shim, J. Meyer, A.J. Giordano, H. Li, P. Winget, T. Papadopoulos, H. Cheun, J. Kim, M. Fenoll, A. Dindar, W. Haske, E. Najafabadi, T.M. Khan, H. Sojoudi, S. Barlow, S. Graham, J.-L. Brédas, S.R. Marder, A. Kahn, B. Kippelen, Science **336**, 327 (2012)
113. C. Duan, C. Zhong, C. Liu, F. Huang, Y. Cao, Chem. Mater. **24**, 1682 (2012)
114. Z. Tan, W. Zhang, Z. Zhang, D. Qian, Y. Huang, J. Hou, Y. Li, Adv. Mater. **24**, 1476 (2012)
115. N. Cho, H.-L. Yip, S.K. Hau, K.-S. Chen, T.-W. Kim, J.A. Davies, D.F. Zeigler, A.K.Y. Jen, J. Mater. Chem. **21**, 6956 (2011)
116. N. Cho, H.-L. Yip, J.A. Davies, P.D. Kazarinoff, D.F. Zeigler, M.M. Durban, Y. Segawa, K. M. O'Malley, C.K. Luscombe, A.K.Y. Jen, Adv. Ener. Mater. **1**, 1148 (2011)
117. C.S. Kim, S. Lee, L.L. Tinker, S. Bernhard, Y.-L. Loo, Chem. Mater. **21**, 4583 (2009)
118. R.-Q. Png, P.-J. Chia, J.-C. Tang, B. Liu, S. Sivaramakrishnan, M. Zhou, S.-H. Khong, H.S. O. Chan, J.H. Burroughes, L.-L. Chua, R.H. Friend, P.K.H. Ho, Nat. Mater. **9**, 152 (2010)
119. P. Wei, J.H. Oh, G. Dong, Z. Bao, J. Am. Chem. Soc. **132**, 8852 (2010)
120. C. Tao, S. Ruan, G. Xie, X. Kong, L. Shen, F. Meng, C. Liu, X. Zhang, W. Dong, W. Chen, Appl. Phys. Lett. **94**, 043311 (2009)
121. J. Meyer, S. Hamwi, S. Schmale, T. Winkler, H.-H. Johannes, T. Riedl, W. Kowalsky, J. Mater. Chem. **19**, 702 (2009)
122. Y. Gao, H.-L. Yip, K.-S. Chen, K.M. O'Malley, O. Acton, Y. Sun, G. Ting, H. Chen, A.K.Y. Jen, Adv. Mater. **2011**, 23 (1903)
123. Y. Gao, H.-L. Yip, S.K. Hau, K.M. O'Malley, N.C. Cho, H. Chen, A.K.Y. Jen, Appl. Phys. Lett. **97**, 203306 (2010)
124. Y.-Y. Lee, K.-H. Tu, C.-C. Yu, S.-S. Li, J.-Y. Hwang, C.-C. Lin, K.-H. Chen, L.-C. Chen, H.-L. Chen, C.-W. Chen, ACS Nano **5**, 6564 (2011)
125. J. Zou, H.-L. Yip, Y. Zhang, Y. Gao, S.-C. Chien, K. O'Malley, C.-C. Chueh, H. Chen, A. K. Y. Jen, Adv. Funct. Mater **22**, 2804 (2012)
126. C. Waldauf, M. Morana, P. Denk, P. Schilinsky, K. Coakley, S.A. Choulis, C.J. Brabec, Appl. Phys. Lett. **89**, 233517 (2006)
127. H. Choi, J.S. Park, E. Jeong, G.-H. Kim, B.R. Lee, S.O. Kim, M.H. Song, H.Y. Woo, J.Y. Kim, Adv. Mater. **23**, 2759 (2011)
128. S.-I. Na, T.-S. Kim, S.-H. Oh, J. Kim, S.-S. Kim, D.-Y. Kim, Appl. Phys. Lett. **97**, 213301 (2010)
129. Y. Sun, J.H. Seo, C.J. Takacs, J. Seifter, A.J. Heeger, Adv. Mater. **23**, 1679 (2011)